Plasmonics in two-dimensional materials: a wave-kinetic description

José Luís Figueiredo[1, 2, *]

[1] *Instituto de Plasmas e Fusão Nuclear, Lisboa, Portugal*
[2] *Instituto Superior Técnico, Lisboa, Portugal*

We derive a quantum kinetic model describing the dynamics of graphene electrons and holes in phase space, based on the Wigner-Moyal procedure. In order to take into account the quantum nature of the carriers, we start from the low-energy Schrödinger equation describing the mean-field wave-function for both the conduction and valence electron. The equation of motion for the Wigner tensor is established, where the Coulomb interaction is introduced self-consistently (in the Hartree approximation), and the Poisson equation closes the set of equations. The long wavelength limit for the plasmon dispersion relation is obtained, in the case of non-zero doping. As an application, we derive the corresponding hydrodynamical equations and discuss the correct value of the effective hydrodynamic mass of the carriers from first principles, an issue that is crucial in the establishment of the correct hydrodynamics of Dirac particles, thus paving the stage towards a more comprehensive description of graphene plasmonics. Moreover, the Wigner-Poisson is used to describe an instability in doped double-layer graphene, when a beam of electrons is injected in one of the layers. We find unstable plasmon solutions with growth rates as high as 20THz for realistic experimental conditions.

I. INTRODUCTION

Graphene is a single layer of sp^2-bonded carbon atoms, which are densely packed in the form of a benzene ring structure [1], which has been extensively studied due to its spectacular optical, electronic and mechanical properties [2]. In addition to its two-dimensional (2D) nature, the elementary electronic excitations are described by a Dirac-like dispersion in the low-energy limit [3]. The relativistic nature of graphene quasi-particles, resulting from the cone-like dispersion relation near the Dirac points, makes it useful for transparent electronic devices, ultrasensitive photodetectors and other high-performance optoelectronic structures [4, 5]. Furthermore, graphene possesses extremely high quantum efficiency for light-matter interactions [6]. Moreover, the collective oscillations of the electron and hole densities lead to the formation of plasmons (or plasma waves) [7]. In fact, plasmonics of 2D materials, such as graphene and transition metal dichalcogenides (TMDCs) and hexagonal boron nitride (hBN) [8, 9], is nowadays a very prominent field of research [10]. Graphene-based plasmonics finds a variety of applications, as the versatility of graphene enables the manufacture of optical devices working in different frequency ranges, namely in the terahertz (THz) and the infra-red domains [11]. While metal plasmonics exhibit large Ohmic losses, which limit their applicability to optical processing devices, doped graphene emerges as an alternative. Its large conductivity, in part due to the zero-mass character of the carriers, encloses a wide range of potential applications, such as high-frequency nanoelectronics, nanomechanics, transparent electrodes, and composite materials [12]. For this reason, the possibility of electric gating has been extensively studied in graphene, allowing for the manipulation of the Fermi level [13]. Recently, gating with a solid electrolyte allowed carrier concentrations as large as 10^{14} cm^{-2} to be achieved, which results in a Fermi energy of $E_F \approx 1$ eV, such that a modulation of optical transmission in the visible spectrum is possible [14, 15]. The potentiality of THz emission was also pointed out [16] as a possible application recently, by making use of a graphene field-effect transistor (gFET), and controlling the applied gate voltage and injected current.

From the theoretical point of view, a variety of techniques have been developed to establish the dynamics of Dirac electrons and holes in graphene, ranging from semiclassical hydrodynamical models [17–19] to quantum formalisms that involve collective Green's functions, such as the time-dependent Hartree-Fock approximation [20, 21], or the time-dependent density functional theory [22]. In one hand, it is often the case that, when going towards a complete quantum description, cumbersome equations crop up, which are of very reduced utility; on the other, the semiclassical approach is based on the Boltzmann equations, which is adequate in the case of dense electron and hole densities, but may fail to describe other important quantum phenomena.

In this work, we establish a kinetic formalism based on the Wigner formulation of quantum mechanics [23] to study the Dirac electrons and holes in phase space. We start by constructing the Schrödinger equation for the conduction and valence electrons, derived from a microscopic tight-binding model, for the low-energy electrons. After moving to the electron-hole basis, we derive a kinetic equation for the Wigner matrix components, which correctly incorporates the pseudo-spin degrees of freedom. The interaction is introduced self-consistently via the Hartree approximation, which obeys the Poisson equation. With this in hand, we are able to obtain the plasmon dispersion relation, recovering the usual result based on the random-phase approximation. By performing averages over the phase-space distributions (more precisely, by taking the moments of the Wigner equa-

* jose.luis.figueiredo@tecnico.ulisboa.pt

tion), hydrodynamical equations are obtained allowing for fluid description of the Dirac particles in graphene. As a consequence, we are able to derive microscopically the effective mass of a fluid particle and relate it to the Drude mass, thus contributing to the understanding of an important question in graphene hydrodynamics. We also show that the classical limit corresponds to previous results based on the Vlasov equation for the classical distribution function. As an application, a type of instability is studied in spatially separated double-layer graphene. When a beam of electrons is injected in one of the layers, unstable plasmon solutions can develop, with real frequencies in the THz-range, and achievable growth rates of tens of THz.

II. GRAPHENE PRELIMINARIES

The SLG lattice is a 2D lattice made out of carbon atoms disposed into two sublattices, A and B. Each unit cell contains two carbon atoms that belong to different sublattices, and each atom is strongly bounded to three other, by a sp^2 hybridization. The remaining valence electron is delocalized, and responsible for most of the electronic properties. The electronic dynamics can be captured starting with an Hamiltonian in second quantization

$$\hat{H} = \sum_{s,s'} \sum_{\boldsymbol{R},\boldsymbol{R'}} \hat{u}_s^\dagger(\boldsymbol{R}) \, \langle \hat{u}_s, \boldsymbol{R} | \hat{H} | \hat{u}_{s'}, \boldsymbol{R'} \rangle \, \hat{u}_{s'}(\boldsymbol{R'}), \tag{1}$$

where $\boldsymbol{R}/\boldsymbol{R'}$ run over the real lattice, and s/s' over the two sublattices A and B. Additionally, $\hat{u}_s^\dagger(\boldsymbol{R})$ and $\hat{u}_s(\boldsymbol{R})$ denote the creation and annihilation operators, respectively, for each lattice point. Moreover, the tight-binding approximation can be settled with a proper restriction on the matrix elements $\langle \hat{u}_s, \boldsymbol{R} | \hat{H} | \hat{u}_{s'}, \boldsymbol{R'} \rangle$. By allowing hopping only between nearest neighbors, we can set all matrix elements to zero except the cases of $\langle \hat{u}_s, \boldsymbol{R} | \hat{H} | \hat{u}_{s'}, \boldsymbol{R} + \boldsymbol{\delta}_i \rangle = -t(1 - \delta_{ss'})$, where t ≈ 2.97 eV is the hopping integral and $\boldsymbol{\delta}_i$ are graphene's nearest-neighbor vectors [3]. In momentum space, the Hamiltonian reduces to

$$\hat{H} = \sum_{\boldsymbol{q}} \boldsymbol{\varphi}_{\boldsymbol{q}}^\dagger \begin{pmatrix} 0 & -t\Delta \\ -t\Delta^* & 0 \end{pmatrix} \boldsymbol{\varphi}_{\boldsymbol{q}}, \tag{2}$$

where $\boldsymbol{q} = (q_x, q_y)$ is the wave-vector, $\boldsymbol{\varphi}_{\boldsymbol{q}} = (\hat{u}_{A\boldsymbol{q}}, \hat{u}_{B\boldsymbol{q}})^T$ and $\Delta(\boldsymbol{q}) = \sum_i e^{-i\boldsymbol{q}\cdot\boldsymbol{\delta}_i}$. We can further diagonalise (2), by the means of a unitary transformation $\boldsymbol{\Phi}(\boldsymbol{q}, t) = S\boldsymbol{\varphi}(\boldsymbol{q}, t)$, where $\boldsymbol{\Phi}^T(\boldsymbol{q}, t) = (\hat{c}_{\boldsymbol{q}} \;\; \hat{v}_{\boldsymbol{q}})$ is a new vector field and $\hat{c}_{\boldsymbol{q}}$ and $\hat{v}_{\boldsymbol{q}}$ are new annihilation operators. We obtain

$$\hat{H} = \sum_{\boldsymbol{q}} \boldsymbol{\Phi}_{\boldsymbol{q}}^\dagger \begin{pmatrix} \hbar\omega(\boldsymbol{q}) & 0 \\ 0 & -\hbar\omega(\boldsymbol{q}) \end{pmatrix} \boldsymbol{\Phi}_{\boldsymbol{q}}, \tag{3}$$

where

$$S = \frac{1}{\sqrt{2}} \begin{pmatrix} -e^{-i\theta(\boldsymbol{q})} & 1 \\ e^{i\theta(\boldsymbol{q})} & 1 \end{pmatrix}, \tag{4}$$

$e^{i\theta(\boldsymbol{q})} = \sqrt{\Delta(\boldsymbol{q})/\Delta^*(\boldsymbol{q})}$, and $\pm\hbar\omega(\boldsymbol{q})$ are the two symmetric energy bands

$$\omega(\boldsymbol{q}) = \frac{t}{\hbar} \sqrt{4\cos\left(\sqrt{3}dq_x/2\right)\cos\left(3dq_y/2\right) + 2\cos\left(\sqrt{3}dq_x\right) + 3}\,. \tag{5}$$

Above, $d \approx 1.5\,\text{Å}$ is the carbon-carbon distance. These energy bands represent the conduction (+) and valence (−) bands for quasi-electrons. Hence, $\hat{c}_{\boldsymbol{q}}^\dagger(\hat{c}_{\boldsymbol{q}})$ creates(annihilates) an electron with momentum $\boldsymbol{q}$ and energy $+\hbar\omega(\boldsymbol{q})$ in the conduction band, and $\hat{v}_{\boldsymbol{q}}^\dagger(\hat{v}_{\boldsymbol{q}})$ creates(annihilates) an electron with momentum $\boldsymbol{q}$ and energy $-\hbar\omega(\boldsymbol{q})$ in the valence band. For energies much smaller than t, we can expand (3) around the Dirac point $\boldsymbol{K} = (4\pi/(3\sqrt{3}d), 0)$ [24], and obtain

$$\omega(\boldsymbol{q}) \simeq v_F|\boldsymbol{q}|, \tag{6}$$

where $v_F = 3\sqrt{3}td/(2h) \approx 10^6$ ms^{-1} is the Fermi velocity As such, the low-energy Hamiltonian in Fourier space yields

$$\hat{H} = \sum_{\boldsymbol{q}} \xi(\boldsymbol{q})\left(\hat{c}_{\boldsymbol{q}}^\dagger \hat{c}_{\boldsymbol{q}} - \hat{v}_{\boldsymbol{q}}^\dagger \hat{v}_{\boldsymbol{q}}\right), \tag{7}$$

where $\xi(\boldsymbol{q}) = \hbar v_F|\boldsymbol{q}|$ is the single-particle dispersion relation near the Dirac point.

By inspecting (7), we still face the problem of treating negative-energy excitations. To circumvent it, we call forth the ground-state of our case of interest. Neutral SLG's ground-state comprises a completely filled valence band and an empty conduction band. Such electronic configuration is known as Fermi Sea, which we denote by $|\Omega_{FS}\rangle$. It is written as

$$|\Omega_{FS}\rangle = \prod_{\boldsymbol{q}\in BZ} \hat{v}_{\boldsymbol{q}}^\dagger \, |0\rangle\,, \tag{8}$$

where $|0\rangle$ is the vacuum state, and BZ is the first Brillouin zone. With this in mind, it is easy to calculate the energy of $|\Omega_{FS}\rangle$, through $\hat{H}\,|\Omega_{FS}\rangle = E_{FS}\,|\Omega_{FS}\rangle$, and realize that $E_{FS} = \sum_{\boldsymbol{q}} -\xi(\boldsymbol{q}) < 0$. Hence, acting on

Ω_{FS} with any $\hat{v}_{\boldsymbol{q}}$ leads to a new state $|\Omega'\rangle$ such that $E_{\Omega'} > E_{FS}$. This implies that destroying a valence electron holds a positive energy excitations to the ground-state, which suggest that the absence of a valence electron (or the presence of a hole in the almost filled Fermi sea) behaves as a positive-energy particle. Therefore, we define two new fermionic creation and annihilation operators $\hat{h}^\dagger_{\boldsymbol{q}}$ and $\hat{h}_{\boldsymbol{q}}$ as $\hat{h}^\dagger_{\boldsymbol{q}} = \hat{v}_{-\boldsymbol{q}}$ and $\hat{h}_{\boldsymbol{q}} = \hat{v}^\dagger_{-\boldsymbol{q}}$, which obey fermionic anti-commutation relations. Physically, $\hat{h}^\dagger_{\boldsymbol{q}}$ creates a hole with momentum $\boldsymbol{q}$ and $\hat{h}_{\boldsymbol{q}}$ destroys a hole with momentum $\boldsymbol{q}$. Since a hole physically corresponds to an unoccupied valence state, it must have a symmetric electric charge, $+e$. In this new basis, we are led to the Hamiltonian

$$\hat{H} = E_{FS} \; + \sum_{\boldsymbol{q}\in BZ} \xi(\boldsymbol{q})\big(\hat{c}^\dagger_{\boldsymbol{q}}\hat{c}_{\boldsymbol{q}} + \hat{h}^\dagger_{\boldsymbol{q}}\hat{h}_{\boldsymbol{q}}\big), \tag{9}$$

which represents a free Hamiltonian for two different species with positive energy, as desired. The constant E_{FS} can be absorbed into $\hat{H}$, and will then be discarded.

We now proceed to find the equation of motion for the two wave-functions of electrons and holes, and further take interactions into account. To do that, let us define the wave-function array $\boldsymbol{\psi}$ as $\boldsymbol{\psi}^T(\boldsymbol{q},t) = (\hat{c}_{\boldsymbol{q}}, \hat{h}_{\boldsymbol{q}})$. We use a Schrödinger type of equation, $i\hbar\partial_t\boldsymbol{\psi} = \hat{H}\boldsymbol{\psi}$, whose Hamiltonian comprises a kinetic term plus a potential, accounting for the Coulomb interaction. In momentum space, it reads

$$i\hbar\frac{\partial}{\partial t}\psi^\alpha(\boldsymbol{q},t) = \xi(\boldsymbol{q})\psi^\alpha(\boldsymbol{q},t) + \int d\boldsymbol{q}'\; V_\alpha(\boldsymbol{q}',t)\psi^\alpha(\boldsymbol{q}-\boldsymbol{q}',t) \tag{10}$$

Above, $V_\alpha(\boldsymbol{q},t)$ is the Fourier transform of the interacting potential. In what follows, we perform our calculations within the Hartree (mean-field) approximation, which boils down to solve the Poisson equation for the electrostatic potential $\phi(\boldsymbol{r},t)$

$$\boldsymbol{\nabla}^2\phi = -\frac{1}{\varepsilon_0\varepsilon_r}\sum_\beta \mathcal{Q}_\beta n_\beta, \tag{11}$$

where $n_\beta(\boldsymbol{r},t) = \big|\psi^\beta(\boldsymbol{r},t)\big|^2$ denotes the electron ($\beta = 1$) and hole ($\beta = 2$) density, $\mathcal{Q}_\beta$ is the charge of the $\beta-$band and $\varepsilon_0\varepsilon_r$ is the permittivity of the surrounding medium. Besides, $V_\alpha(\boldsymbol{r},t)$ is related to $\phi(\boldsymbol{r},t)$ via

$$V_\alpha(\boldsymbol{r},t) = \mathcal{Q}_\alpha\phi(\boldsymbol{r},t), \tag{12}$$

A formal solution to (11) can be written as

$$\phi(\boldsymbol{r},t) = \frac{1}{4\pi\varepsilon_0\varepsilon_r}\int d\boldsymbol{r}'\; \sum_\beta \frac{\mathcal{Q}_\beta n_\beta(\boldsymbol{r}',t)}{|\boldsymbol{r}-\boldsymbol{r}'|}. \tag{13}$$

Equation (13) provides a closure relation to the system of (10), by relating the potential with the electron and hole densities, which in turn are related to the wave-functions. In other words,

$$\phi(\boldsymbol{q},t) = \mathcal{U}(\boldsymbol{q})\sum_\beta\; s_\beta n_\beta(\boldsymbol{q},t), \tag{14}$$

where $\mathcal{U}(\boldsymbol{q}) = e/2\varepsilon_0\varepsilon_r|\boldsymbol{q}|$ is the Fourier transform of the Coulomb interaction term, in 2D, and $s_\alpha = 2\alpha - 3$ is the sign of the $\alpha-$charge.

III. WIGNER FORMALISM

A very handy way to treat the electronic system of (10) is by using Wigner's picture of quantum mechanics [23], which allows for a fully phase-space description, in close analogy with the classical case. In the classical limit, the Wigner function denotes the probability density of finding a particle in a given infinitesimal phase space volume $d\boldsymbol{r}\; d\boldsymbol{k}$ centred in $(\boldsymbol{r},\boldsymbol{k})$. In the quantum case, due to the commutation relation between $\boldsymbol{r}$ and $\boldsymbol{q}$, the Heisenberg uncertainty principle prevents particles to localize in a specific phase-space point, and a proper distribution function is not possible to construct [25]. However, we can still construct the Wigner function $W(\boldsymbol{r},\boldsymbol{k},t)$ whose properties are similar to those of a classical distribution function. It is a function of both a spatial coordinate $\boldsymbol{r}$ and a wave-vector coordinate $\boldsymbol{k}$. Although $\boldsymbol{r}$ and $\boldsymbol{k}$ are not conjugate to each other, they both give information about the spatial and momentum distributions of the system, which is described by a wave-function $\psi(\boldsymbol{r},t)$. The phase-space regions where $W(\boldsymbol{r},\boldsymbol{k},t)$ takes negative values are purely quantum, having no classical analogue as it cannot be univocally defined as a particle phase-space density. For that reason, the Wigner function is often refereed to as a quasi-distribution function. The mathematical definition of the Wigner function is given by the Weyl transform of the density operator $\hat{\rho}$. The expectation values of any operator can be computed by integrating the Weyl transform of the same operator multiplied by $W(\boldsymbol{r},\boldsymbol{k},t)$, very similarly to the classical case. For the present case, it is given by a tensor $W^{\alpha\gamma}(\boldsymbol{r},\boldsymbol{k},t)$, accounting for the pseudo-spin degrees of freedom, and is defined as

$$W^{\alpha\gamma}(\boldsymbol{r},\boldsymbol{k},t) = \int \frac{d\boldsymbol{s}}{(2\pi)^2}\; e^{i\boldsymbol{k}\cdot\boldsymbol{s}} \times \psi^\alpha(\boldsymbol{r}-\boldsymbol{s}/2,t)\; \psi^{*\gamma}(\boldsymbol{r}+\boldsymbol{s}/2,t). \tag{15}$$

The tensorial structure renders an Hermitian Wigner matrix, rather than their components being all real, as in the conventional scalar case. Although the diagonal terms are still real, the off-diagonal elements can have non-zero imaginary parts, despite being complex conjugate of each other. Those elements represent the density correlations between the two populations. Notwithstanding, in the present mean-field approximation, the off-diagonal terms totally decouple from the system, and evolve independently. On the other hand, the diagonal elements

are linked through the interacting potential, as they represent the density of each population. If one considers higher order terms on the electron-electron interaction (*e.g.*, by taking into account exchange effects), the off-diagonal elements would no longer be discarder. As such, we have (no implicit summation is implied)

$$n_\alpha(\boldsymbol{r},t) = \int d\boldsymbol{k}\; W^{\alpha\alpha}(\boldsymbol{r},\boldsymbol{k},t)\;. \tag{16}$$

In momentum space, Eq. (15) transforms to

$$W^{\alpha\gamma}(\boldsymbol{q},\boldsymbol{k},t) = \psi^{\alpha}(\boldsymbol{k}+\boldsymbol{q}/2,t)\;\psi^{*\gamma}(\boldsymbol{k}-\boldsymbol{q}/2,t) \tag{17}$$

To construct an equation for the Wigner matrix elements, we start by writing (10) and its hermitian conjugate for two independent momentum coordinates, $\boldsymbol{q}_1$ and $\boldsymbol{q}_2$, and distinct band indices, α and γ. By multiplying the fist by $\psi^{*\gamma}(\boldsymbol{q}_2,t)$ and the second by $\psi^{\alpha}(\boldsymbol{q}_1,t)$ and subtracting the results, we arrive at

$$\begin{aligned} i\hbar\frac{\partial}{\partial t}\Big[\psi^{\alpha}(\boldsymbol{q}_1,t)\psi^{*\gamma}(\boldsymbol{q}_2,t)\Big] &= \Big[\xi(\boldsymbol{q}_1)-\xi(\boldsymbol{q}_2)\Big]\psi^{\alpha}(\boldsymbol{q}_1,t)\psi^{*\gamma}(\boldsymbol{q}_2,t) \\ &+\int d\boldsymbol{q}'\Big[V_\alpha(\boldsymbol{q}',t)\psi^{\alpha}(\boldsymbol{q}_1-\boldsymbol{q}',t)\psi^{*\gamma}(\boldsymbol{q}_2,t) - V_\gamma(\boldsymbol{q}',t)\psi^{\alpha}(\boldsymbol{q}_1,t)\psi^{*\gamma}(\boldsymbol{q}_2-\boldsymbol{q}',t)\Big], \end{aligned} \tag{18}$$

where we used $V_\alpha(\boldsymbol{q}',t)^* = V_\alpha(-\boldsymbol{q}',t)$. Recalling the identity $f(\boldsymbol{k}+\boldsymbol{q}) = e^{\boldsymbol{q}\cdot\boldsymbol{\nabla}_k}f(\boldsymbol{k})$, and introducing the coordinate transformation $\boldsymbol{q}_1 = \boldsymbol{k}+\boldsymbol{q}/2$, $\boldsymbol{q}_2 = \boldsymbol{k}-\boldsymbol{q}/2$, (18) it follows, after some straightforward algebra

$$\Big[i\hbar\;\frac{\partial}{\partial t} - \Delta\xi^{-}(\boldsymbol{q},\boldsymbol{k})\Big]W^{\alpha\gamma}(\boldsymbol{q},\boldsymbol{k},t) = e\int d\boldsymbol{q}'\;\phi(\boldsymbol{q}',t) \times \Delta W^{\alpha\gamma}(\boldsymbol{q},\boldsymbol{k},\boldsymbol{q}',t), \tag{19}$$

where $\Delta W^{\alpha\gamma}(\boldsymbol{q},\boldsymbol{k},\boldsymbol{q}',t) = s_\alpha W^{\alpha\gamma}(\boldsymbol{q}-\boldsymbol{q}',\boldsymbol{k}-\boldsymbol{q}'/2,t) - s_\gamma W^{\alpha\gamma}(\boldsymbol{q}-\boldsymbol{q}',\boldsymbol{k}+\boldsymbol{q}'/2,t)$ and $\Delta\xi^{-}(\boldsymbol{q},\boldsymbol{k}) = \xi(\boldsymbol{k}+\boldsymbol{q}/2) - \xi(\boldsymbol{k}-\boldsymbol{q}/2)$. Equation (19) and (14) define the Wigner-Poisson model for 2D Dirac particles, in Fourier space. For the diagonal components $W^{\alpha\alpha}(\boldsymbol{r},\boldsymbol{k},t) \doteq W^{\alpha}$, the real space Wigner equation (19) reads

$$i\hbar\frac{\partial}{\partial t}W^{\alpha} + i\hbar\mathcal{K}\{W^{\alpha}\} = \int d\boldsymbol{q}\; e^{i\boldsymbol{q}\cdot\boldsymbol{r}}\;\left(W^{\alpha}_{-} - W^{\alpha}_{+}\right) \times V_\alpha(\boldsymbol{q},t), \tag{20}$$

where $W^{\alpha}_{\pm} \doteq W^{\alpha}(\boldsymbol{r},\boldsymbol{k}\pm\boldsymbol{q}/2,t)$ and

$$\mathcal{K}\{W^{\alpha}\} = v_F\int\frac{d\boldsymbol{r}'}{(2\pi)^2}\frac{\sin\left(2\boldsymbol{k}\cdot\boldsymbol{r}\right)}{|\boldsymbol{r}|^3}\;W^{\alpha}(\boldsymbol{r}-\boldsymbol{r}',\boldsymbol{k},t), \tag{21}$$

represents the kinetic term, for which no classical limit exists. This defining difference confers to Dirac particles a purely quantum nature.

In what follows, we consider small perturbations around an equilibrium configuration, keeping the lowest order contributions to the Wigner function components. As such, we can write

$$W^{\alpha\gamma}(\boldsymbol{r},\boldsymbol{k},t) \simeq W^{\alpha}_0(\boldsymbol{k})\delta^{\alpha\gamma} + \tilde{W}^{\alpha\gamma}(\boldsymbol{r},\boldsymbol{k},t), \tag{22}$$

with $|\tilde{W}^{\alpha\gamma}| \ll W^{\alpha}_0$, which in momentum space reads $W^{\alpha\gamma}(\boldsymbol{q},\boldsymbol{k},t) \simeq W^{\alpha}_0(\boldsymbol{k})\delta(\boldsymbol{q})\delta^{\alpha\gamma} + \tilde{W}^{\alpha\gamma}(\boldsymbol{q},\boldsymbol{k},t)$. Similarly, the density and electrostatic potential will be perturbed as

$$n_\alpha(\boldsymbol{q},t) \simeq n^{\alpha}_0\delta(\boldsymbol{q}) + \tilde{n}_\alpha(\boldsymbol{q},t), \tag{23}$$

$$\phi(\boldsymbol{q},t) \simeq \mathcal{U}(\boldsymbol{q})\sum_\beta\left[n_0\delta(\boldsymbol{q}) + \tilde{n}_\beta(\boldsymbol{q},t)\right], \tag{24}$$

where $n^{\alpha}_0 = \int d\boldsymbol{k}W^{\alpha}_0(\boldsymbol{k})$ is the equilibrium density of each band. We can show that the lowest order contributions of (19) vanish. Moreover, the first order terms provide

$$i\hbar\frac{\partial}{\partial t}\tilde{W}^{\alpha\gamma}(\boldsymbol{q},\boldsymbol{k},t) = \Delta\xi^{-}(\boldsymbol{q},\boldsymbol{k})\tilde{W}^{\alpha\gamma}(\boldsymbol{q},\boldsymbol{k},t) + \sum_\beta\tilde{n}_\beta(\boldsymbol{q},t) \times \mathcal{Q}_\alpha\mathcal{U}(\boldsymbol{q})\Delta W^{\alpha}_0(\boldsymbol{k},\boldsymbol{q})\delta^{\alpha\gamma} \tag{25}$$

where $\Delta W_0(\boldsymbol{k}) = W_0(\boldsymbol{k}-\boldsymbol{q}/2) - W_0(\boldsymbol{k}+\boldsymbol{q}/2)$. Equation (25) is formally equivalent to Kubo's formula for the linear response of a many-body charged system [26], and reproduces the features contained in the random phase approximation (RPA) [27]. This formalism is specially advantageous to describe the dynamics of electrons that are far from equilibrium, such as the case of plasma instabilities, with the configuration being solely defined by W_0.

In what follows, we consider the case of SLG doped with negative charge carriers, which occupy the conduction band. In this configuration, the conduction band gets filled up with electrons up to the Fermi level, E_F. In momentum-energy space, this is defined by the cone $E(\boldsymbol{k}) = \hbar v_F|\boldsymbol{k}|\Theta(k_F - |\boldsymbol{k}|)$, where $\Theta(x)$ is the Heaviside step function, and $k_F = E_F/(\hbar v_F)$ is the Fermi wavenumber. The latter is related to the doping density n_0 by

$$k_F = \sqrt{\frac{4\pi n_0}{g_s g_v}}, \tag{26}$$

where $g_s g_v$ accounts for the spin ($g_s = 2$) and valley ($g_v = 2$) degeneracy. The first results from the degeneracy of the spin populations in each energy band, which

we have neglected in our treatment so far; the second should be incorporated to consistently include the two minima in the first Brillouin zone (BZ) [28]. Typical experimental values of n_0 between $10^9 - 5\times10^{12}$ cm^{-2} are achievable in graphene. In the case $E_F \gg k_BT$, the presence of holes is negligible, and the first component of (19) is sufficient. Hence, to simplify the notation, we shall drop the band indices, $W \doteq W^{11}$ and $n \doteq n_1$. We can solve the first component of (19) equation perturbatively, for the plasmon dispersion relation, which leads to the allowed frequencies ω for each mode $\boldsymbol{q}$ of the plasma wave, of the form $\omega = \omega(\boldsymbol{q})$. After Fourier transforming the time coordinate, we can recast (25) into a more familiar form. Straightforward manipulation leads to

$$\tilde{W}(\boldsymbol{q},\boldsymbol{k},\omega) = \tilde{n}(\boldsymbol{q},\omega)\,\mathcal{U}(\boldsymbol{q})\,\frac{\Delta W_0(\boldsymbol{k},\boldsymbol{q})}{\hbar\omega - \xi(\boldsymbol{k}+\boldsymbol{q}/2)+\xi(\boldsymbol{k}-\boldsymbol{q}/2)}. \tag{27}$$

Upon integrating both sides in $\boldsymbol{k}$, we find the dielectric function $\epsilon(\boldsymbol{q},\omega)$

$$\epsilon(\boldsymbol{q},\omega) = 1 - \mathcal{U}(\boldsymbol{q})\Pi(\boldsymbol{q},\omega), \tag{28}$$

and the polarizability function $\Pi(\boldsymbol{q},\omega)$ is defined as

$$\Pi(\boldsymbol{q},\omega) = \int d\boldsymbol{k}\;\frac{W_0(\boldsymbol{k}) - W_0(\boldsymbol{k}+\boldsymbol{q})}{\hbar\omega + \xi(\boldsymbol{k}) - \xi(\boldsymbol{k}+\boldsymbol{q})}. \tag{29}$$

The plasmon dispersion relation is given by the zeros of $\epsilon(\boldsymbol{q},\omega)$. We note that, in the absence of streaming, $\epsilon(\mathbf{q},\omega)$ and $\omega(\mathbf{q})$ depends only on $q \equiv |\mathbf{q}|$. The formal result of Eq. (28) is equivalent to the random-phase approximation (RPA) [29]. In the long wavelength limit $q \to 0$, the plasmon frequency can be computed using the noninteracting irreducible polarizability, and Eq. (28) is recovered. We assume the equilibrium configuration to be given by

$$W_0(\boldsymbol{k}) = n_0\Theta(k_F - k)/\pi k_F^2. \tag{30}$$

This is justified invoking the 2D Fermi model for an electron gas since, in the ultra-cold limit $T \to 0$, we have $\lim_{T\to0} f_{FD}(\xi_{\boldsymbol{k}}) = \Theta(E_F - \xi_{\boldsymbol{k}})$. $f_{FD}(x)$ denotes the Fermi-Dirac distribution function. Additionally, (30) verifies $\int d\boldsymbol{k}\; W_0(\boldsymbol{k}) = n_0$. Note that the correct form of $f_{FD}(\xi_{\boldsymbol{k}})$ can be introduced as temperature corrections to the Heaviside step function used above, which are found to be negligible in the present case. Expanding (28) around $q = 0$, and keeping only terms up to $\mathcal{O}(q^2)$, the plasmon dispersion relation is obtained

$$\omega(q) = \pm\Big(\omega_p^2\frac{q}{k_F} + \frac{3}{4}v_F^2q^2\Big)^{1/2}, \tag{31}$$

where ω_p is the characteristic plasmon frequency

$$\omega_p = \left(\frac{e^2n_0v_F}{2\hbar\varepsilon_0\varepsilon_r}\right)^{1/2}, \tag{32}$$

which depends on experimental parameters ε_r and n_0, as well as universal constants. Each branch corresponds to a different direction of propagation (forward and backward waves) for longitudinal plasmonic modes. For the typical experimental values $\varepsilon_r = 2.5$ and $n_0 \in [5\times10^{-3}, 1]\times10^{12}$ cm^{-2}, ω_p lies in the THz-region, $\omega_p \in [16.6, 234.6]$ THz. The first term $\omega \sim \sqrt{q}$ describes the long wavelength signature of plasmons in two-dimensional electron gases (2DEG) [30, 31]. The most notable difference, when compared to the characteristic plasmon frequency in the 3-dimensional parabolic case, $\omega_p^{3D} = \sqrt{e^2n_0/(\varepsilon_0 m)}$, is the appearance of $\hbar$ in the leading term, revealing its pure quantum nature and being a feature of the present quasi-relativistic description. Therefore, no classical counterpart exists for the 2-dimensional Dirac plasma. This result was already found in the literature [32], derived within the RPA.

IV. HYDRODYNAMICAL MODEL

One of the major advantages of the present description is the possibility of calculate the moments out of (19), and thus construct hydrodynamical models. Similarly to the classical case, Wigner's formalism allows the calculation of average quantities in terms of phase-space integrations, and hence obtaining equations which govern the evolution of those quantities. Because we are concerned with the diagonal elements of the Wigner matrix only, we defined W^α as being the diagonal components, *i.e.*, $W^\alpha \doteq W^{\alpha\alpha}$. Similarly to the classical, let us define the average value of an operator $\hat{\mathcal{G}}$ as

$$\overline{\mathcal{G}}_\alpha = \frac{1}{n_\alpha(\boldsymbol{r},t)}\int d\boldsymbol{k}\;\mathcal{T}\{\hat{\mathcal{G}}\}W^\alpha(\boldsymbol{r},\boldsymbol{k},t) \tag{33}$$

where $\mathcal{T}\{\hat{\mathcal{G}}\}$ denotes the Weyl transform of the operator $\hat{\mathcal{G}}$,

$$\mathcal{T}\{\hat{\mathcal{G}}\} = \int\frac{d\boldsymbol{s}}{(2\pi\hbar)^d}\;e^{i\boldsymbol{s}\cdot\boldsymbol{p}/\hbar}\;\langle\boldsymbol{r}-\boldsymbol{s}/2|\hat{\mathcal{G}}|\boldsymbol{r}+\boldsymbol{s}/2\rangle\,. \tag{34}$$

The cases $\hat{\mathcal{G}} = 1$ and $\hat{\boldsymbol{\mathcal{G}}} = \hbar\hat{\boldsymbol{k}}$ define the relevant hydrodynamical variables

$$n_\alpha(\boldsymbol{r},t) = \int d\boldsymbol{k}\;W^\alpha(\boldsymbol{r},\boldsymbol{k},t), \tag{35}$$

$$\overline{\boldsymbol{p}}_\alpha(\boldsymbol{r},t) = \frac{1}{n_\alpha(\boldsymbol{r},t)}\int d\boldsymbol{k}\;\hbar\boldsymbol{k}\;W^\alpha(\boldsymbol{r},\boldsymbol{k},t). \tag{36}$$

Above, we used $\mathcal{T}\{\hat{\boldsymbol{k}}\} = \boldsymbol{k}$.

After differentiating (35) and (36) with respect to time, and use (19) to express the time derivative of the Wigner matrix components, we are led to the hydrodynamical set of equations

$$i\hbar\frac{\partial}{\partial t}n_\alpha = 2\int d\boldsymbol{k}\; d\boldsymbol{q}\; e^{i\boldsymbol{r}\cdot\boldsymbol{q}}\left[\sinh\Big(\frac{\boldsymbol{q}}{2}\cdot\boldsymbol{\nabla}_{\boldsymbol{k}}\Big)\xi(\boldsymbol{k})\right] W^\alpha(\boldsymbol{q},\boldsymbol{k},t), \tag{37}$$

$$\frac{\partial}{\partial t}(n_\alpha\overline{\boldsymbol{p}}_\alpha) = -2i\int d\boldsymbol{k}\; d\boldsymbol{q}\; e^{i\boldsymbol{r}\cdot\boldsymbol{q}}\;\boldsymbol{p}\left[\sinh\Big(\frac{\boldsymbol{q}}{2}\cdot\boldsymbol{\nabla}_{\boldsymbol{k}}\Big)\xi(\boldsymbol{k})\right] W^\alpha(\boldsymbol{q},\boldsymbol{k},t) - \mathcal{Q}_\alpha n_\alpha\boldsymbol{\nabla}\phi. \tag{38}$$

Equations (37) and (38) are valid under the assumptions that the relevant quantities are slow-varying in both space and time, which is the natural requirement to go from a microscopic field theory to a macroscopic hydrodynamical model (coarse-graining condition). The fluid description is only relevant for regimes where changes in macroscopic quantities take place on a much slower spatial and temporal scale than the characteristic scales k_F and ω_p, respectively. This requirement is fulfilled if the characteristic time of the kinematic processes, $t\sim 1/\omega$, is much longer than the inverse collision frequency, $1/\nu_c$, and the typical length L is much greater than the mean free path $l\sim v_F/\nu_c$, so that the plasma can be regarded locally as in a quasi-equilibrium configuration. However, due to the quantum nature of the model, we were able to capture the relativistic Dirac structure in a rigorous way. Actually, in the context of 2D quantum plasmas realized in semiconductor structures, the De Broglie wavelength is replaced by the Thomas-Fermi screening length $\lambda_{\rm TF} = \sqrt{g_s g_v n_0}e^2/(\sqrt{4\pi}\epsilon\hbar v_F)$. This is the analogue of the classical Debye length in plasmas, and differs from the Fermi wavelength defined above, $\lambda_F = 2\pi/k_F$ (ranging as $\sim 10\ \text{nm} - 10\mu\text{m}$ for typical graphene parameters). Consequently, the hydrodynamical limit is expected to be valid provided the condition

$$q\lambda_{\rm TF}\ll 1, \quad q\lambda_F\ll 1. \tag{39}$$

In graphene, $\lambda_F/\lambda_{\rm TF}\simeq 3.2$, such that later condition is the most determinant of validity. Typical values of k_F are found between 10^3 and 10^6 cm^{-1}. At smaller wavelengths, the microscopic structure becomes important, and we no longer can rely on the hydrodynamical model.

A. Classical and semi-classical limits

In order to clarify the meaning of some of the terms in (37) and (38), it is instructive to obtain the classical limit $\hbar\to 0$, which can be done by replacing $\boldsymbol{k}$ with $\boldsymbol{p}/\hbar$ and neglecting $\mathcal{O}(\hbar)$ terms. The semi-classical limits are derived by keeping higher orders of $\hbar$. Taylor expanding the sinh operator in (37) and (38) yields

$$\frac{\partial}{\partial t}n^\alpha + \boldsymbol{\nabla}\cdot\overline{\boldsymbol{j}}_\alpha = \hbar\int d\boldsymbol{k}\;\mathcal{N}\{W^\alpha\}, \tag{40}$$

$$\frac{\partial}{\partial t}n_\alpha\overline{\boldsymbol{p}}_\alpha + \boldsymbol{\nabla}P_\alpha + \mathcal{Q}_\alpha n_\alpha\boldsymbol{\nabla}\phi = \hbar\int d\boldsymbol{k}\;\boldsymbol{p}\;\mathcal{N}\{W^\alpha\}, \tag{41}$$

where $\overline{\boldsymbol{j}}_\alpha = n_\alpha\overline{\boldsymbol{v}}_\alpha$ is the density current, $\overline{\boldsymbol{v}}_\alpha$ is the velocity field

$$\overline{\boldsymbol{v}}_\alpha(\boldsymbol{r},t) = \frac{v_F}{n_\alpha}\int d\boldsymbol{k}\;\frac{\boldsymbol{k}}{|\boldsymbol{k}|}\;W^\alpha(\boldsymbol{r},\boldsymbol{k},t), \tag{42}$$

and P_α is the pressure-tensor

$$P_\alpha(\boldsymbol{r},t) = v_F\int d\boldsymbol{k}\;\frac{1}{|\boldsymbol{p}|}\begin{pmatrix} p_x^2 & p_xp_y\\ p_yp_x & p_y^2\end{pmatrix} W^\alpha(\boldsymbol{r},\boldsymbol{k},t). \tag{43}$$

Equation (42) is what one expects, for massless Dirac particles with constant Fermi velocity. However, the quasi-relativistic nature of the kinetic term in (19) introduces extra quantum contributions ($\mathcal{N}$), which are not present in the conventional parabolic case, and read

$$\mathcal{N}\{W^\alpha\} = -\sum_{n=1}^{+\infty}\frac{2i\hbar^{2n-1}}{(2n+1)!}\int d\boldsymbol{q}\;e^{i\boldsymbol{q}\cdot\boldsymbol{r}}\;W^\alpha(\boldsymbol{q},\boldsymbol{k},t) \times\Big(\frac{\boldsymbol{q}}{2}\cdot\boldsymbol{\nabla}_{\boldsymbol{p}}\Big)^{2n+1}\xi(\boldsymbol{p}). \tag{44}$$

Note that, for parabolic dispersion relation, $\xi(\boldsymbol{p}) = \boldsymbol{p}^2/2m$, $\mathcal{N}$ vanishes. In the massless case, all order derivatives of $\xi(\boldsymbol{p})$ exist. By letting $\hbar\to 0$, we obtain the classical limit of (40) and (41), which is simply their LHS's equaled to zero. Up to this point, we have just considered the density and averaged momentum as hydrodynamical variables. Higher order variables could be defined, being the averaged energy density $n_\alpha\overline{\xi}_\alpha$ the next in the chain, for which new transport equations would be settled, coupling the new to the previous variables. However, within the current scope, equations (40) and (41) suffice to describe the system accurately, as they form a closed set, thus higher order equations in the hydrodynamical hierarchy will be discarded.

To go beyond the classical limit, we can include the first quantum correction in the above equations, by considering the first term of $\mathcal{N}\{W^\alpha\}$, which leads to a semi-classical hydrodynamical model. Therefore, neglecting $\mathcal{O}(\hbar^2)$ terms in (44), we obtain the modified hydrodynamical equations

$$\frac{\partial}{\partial t}n_\alpha + \boldsymbol{\nabla}\cdot\overline{\boldsymbol{j}}_\alpha = \frac{\hbar^2}{24}\Bigg[\frac{\partial^3}{\partial x^3}\Big(n_\alpha\overline{J_{xxx}}_\alpha\Big) + \frac{\partial^3}{\partial y^3}\Big(n_\alpha\overline{J_{yyy}}_\alpha\Big) + 3\frac{\partial^2}{\partial x^2}\frac{\partial}{\partial y}\Big(n_\alpha\overline{J_{xxy}}_\alpha\Big) + 3\frac{\partial^2}{\partial y^2}\frac{\partial}{\partial x}\Big(n_\alpha\overline{J_{yyx}}_\alpha\Big)\Bigg], \tag{45}$$

$$\frac{\partial}{\partial t}(n_\alpha \overline{\boldsymbol{p}}_\alpha) + \boldsymbol{\nabla} P_\alpha + \mathcal{Q}_\alpha n_\alpha \boldsymbol{\nabla}\phi = \frac{\hbar^2}{24}\Bigg[\frac{\partial^3}{\partial x^3}\left(n_\alpha \overline{\boldsymbol{T}_{xxx}}_\alpha\right) + \frac{\partial^3}{\partial y^3}\left(n_\alpha \overline{\boldsymbol{T}_{yyy}}_\alpha\right) + 3\frac{\partial^2}{\partial x^2}\frac{\partial}{\partial y}\left(n_\alpha \overline{\boldsymbol{T}_{xxy}}_\alpha\right) + 3\frac{\partial^2}{\partial y^2}\frac{\partial}{\partial x}\left(n_\alpha \overline{\boldsymbol{T}_{yyx}}_\alpha\right)\Bigg], \tag{46}$$

where we defined the new dispersive tensors J_{ijl} and $\boldsymbol{T}_{ijl}$ as

$$J_{ijl} = v_F\left(\frac{3p_ip_jp_l}{|\boldsymbol{p}|^5} - \frac{\delta_{ij}p_l + \delta_{jl}p_i + \delta_{li}p_j}{|\boldsymbol{p}|^3}\right), \tag{47}$$

$$\boldsymbol{T}_{ijl} = \boldsymbol{p}J_{ijl}. \tag{48}$$

B. Mass transport

Having set the relevant transport equations, we shall move now to a more detailed discussion concerning the averaged momentum and velocity fields. To start this discussion on the scope of the present work, let us start by considering the pure electron case, for which we shall drop the band index α, to condense notation. As one can easily conclude by comparing the definitions of (36) and (42), the usual relation $\overline{\boldsymbol{p}} = m\overline{\boldsymbol{v}}$ does not hold, in the present case of massless Dirac particles [33], if one requires a constant value of m. However, by allowing a space and time dependence on the mass, we are able to define a new mass-tensor as

$$m_{ij}(\boldsymbol{r},t) = \frac{\overline{p}_i}{\overline{v}_i}\delta_{ij}, \tag{49}$$

as well as the mass density tensor $\rho_{ij} = nm_{ij}$. The meaning of such fields should be clear: despite the charge carriers have no mass, *i.e.*, they are described by a Dirac-type of equation, the fluid velocity and momentum fields can be used to construct a fictitious mass, simply by dividing one by the other, motivated by the usual parabolic case. Nevertheless, the value of the mass at each point in space and time does not correspond to the actual mass of carriers, but rather to what would the mass be if the two fields were indeed proportional to each other. It should, thus, be interpreted as a mathematical trick to provide more handy equations. Moreover, the tensorial structure for the mass should be included to contemplate the most generic case, for which the rotational symmetry in real space can be broken. However, up to this point, no rotational-symmetry breaking terms were included, and m_{ij} should, thus, become proportional to the identity matrix, *i.e.*, $m_{ij}(\boldsymbol{r},t) = m(\boldsymbol{r},t)\delta_{ij}$.

In order to eliminate the velocity tensor for the continuity equations, we modify the equilibrium Wigner function used in the last chapter, to contemplate an adiabatic non-equilibrium situation. As such, we can assume the Wigner diagonal component $W^\alpha \doteq W$ to be given generically by

$$W(\boldsymbol{r},\boldsymbol{k},t) = \frac{n_0}{\pi k_F^2}\Theta\left(k_F - n_0\left|\frac{\boldsymbol{k}-\overline{\boldsymbol{k}}(\boldsymbol{r},t)}{n(\boldsymbol{r},t)}\right|\right), \tag{50}$$

which represents a shifted Fermi sphere in momentum space, modeled by the hydrodynamical variables n and $\overline{\boldsymbol{k}}$. This particular form for the Wigner function allows (35) and (36) to be exactly satisfied. Introducing (50) into the $x-$component of (42) leads to

$$\overline{v}_x(\boldsymbol{r},t) = \frac{\overline{p}_x(\boldsymbol{r},t)}{\mathcal{M}\gamma(\boldsymbol{r},t)}, \tag{51}$$

where $\mathcal{M} = \hbar k_F/v_F$ is the Drude mass, and γ is the quasi-relativistic Lorentz factor

$$\gamma^{-1}(n,\overline{p}_x) = \frac{8}{\pi}\int_0^1 dy\ \frac{\sqrt{1-y^2}}{\sqrt{f_+}+\sqrt{f_-}}\ , \tag{52}$$

$$f_\pm = \left(p' \pm n'\sqrt{1-y^2}\right)^2 + y^2,\ p' = \frac{\overline{p}_x}{p_F},\ n' = \frac{n}{n_0}.$$

Hence, γ depends on the position and time merely through the hydrodynamical variables $n(\boldsymbol{r},t)$ and $\overline{p}_x(\boldsymbol{r},t)$. Although the integral of (52) has no analytic solution, it reduces to simple expressions, in the limiting cases of small and large average momentum. We can verify that $(\partial\gamma/\partial\overline{p}_x)_{\overline{p}_x=0} = 0$, thus in the limit of small fluid momentum $\overline{p}_x/p_F \ll 1$, γ becomes momentum independent, as

$$\gamma(n) \simeq \frac{\pi}{4}\ \frac{1-n^2/n_0^2}{K_1(1-n^2/n_0^2) - K_2(1-n^2/n_0^2)}, \tag{53}$$

where $K_1(x)$ and $K_2(x)$ are the complete elliptic integrals of the first and second kind, respectively, $K_1(x) = \int_0^{\pi/2} d\theta\ (1-x^2\sin^2\theta)^{-1/2}$ and $K_2(x) = \int_0^{\pi/2} d\theta\ (1-x^2\sin^2\theta)^{1/2}$. Accordingly, the quantities $\overline{p}_x$ and $\overline{v}_x$ become proportional to each other, ensuring a relation of the form $\overline{p}_x = m(n)\overline{v}_x$. However, only for the case $n = n_0$ the mass converges to the Drude mass, *i.e.*, the asymptotic expression of (53) verifies $\gamma(n_0) = 1$. For general out-of-equilibrium conditions with small averaged momentum, we have $m(n) = \gamma(n)\mathcal{M}$. For the limiting case of $\overline{p}_x/p_F \gg 1$, thus keeping only $\mathcal{O}(p_F/\overline{p}_x)$ terms in (52), we find $\gamma \simeq |\overline{p}_x|/(v_F\mathcal{M})$. This implies $\overline{v}_x \simeq v_F\ sign(\overline{p}_x)$, where $sign(x)$ returns the sign of x. Then, for large fluid momentum, the fluid velocity approaches the Fermi velocity, never overcoming it, and becomes independent of the density and absolute value of $\overline{p}_x$, retaining only the momentum sign. In Fig. 1, we can see how changes on the density affect this relation. For increasing values of the density, the region of linearity becomes larger. On the contrary, for vanishingly small density, the relation is rapidly non-linear with increasing $\overline{p}_x$.

We should also comment on the particular choice of (50). The incompressibility of the phase-space fluid, in

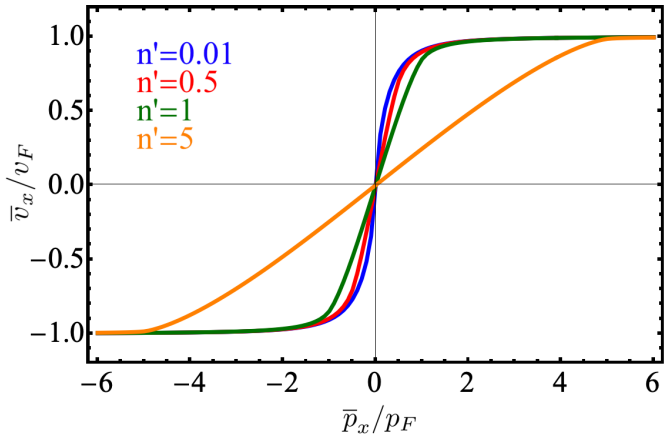

FIG. 1. Numerical integration of (52), for several values of the normalised density n'. Near the origin, we find a linear relation, while for large momentum, the velocity converges, in absolute value, to the Fermi velocity, becoming only a function of the sign of $\overline{p}_x$.

a quantum picture, is violated by phenomena like tunneling, which would lead to a change in the amplitude of W, along a particle's trajectory. Such behaviour is clearly not casted by (50). Nevertheless, (50) is correct to first order, and gets more accurate as the temperature decreases.

C. Semi-classical dispersion relation

Next, we give analytical expressions for (43), (47) and (48), in terms of the previous hydrodynamical variables n_α and $\overline{\boldsymbol{p}}_\alpha$, using (50). We restrict, yet again, the variations to the $x-$direction, such that the relevant quantities are J_{xxx}, T^x_{xxx} and P_{xx}, and the remaining ones can be discarded. In what follows, we intend to derive the linearised version of the hydrodynamical equations, for which we introduce the expansions $n(x,t) = n_0 + \tilde{n}(x,t)$ and $\overline{p}_x(x,t) = \overline{p}_{x,0} + \tilde{\overline{p}}_x(x,t)$. Neglecting second order terms, the relevant components featuring the hydrodynamical equations read

$$\overline{J_{xxx}} \simeq -\frac{3v_F}{4p_F^3}\tilde{\overline{p}}_x, \tag{54}$$

$$\overline{T^x_{xxx}} \simeq \frac{3v_F}{p_F}\left(\frac{1}{4} - \frac{1}{8}\frac{\tilde{n}}{n_0}\right), \tag{55}$$

$$P_{xx} \simeq p_F v_F n_0 \left(\frac{1}{3} + \frac{3}{4}\frac{\tilde{n}}{n_0}\right), \tag{56}$$

Up to first order, the velocity is related to the momentum by

$$\overline{v}_x \simeq \frac{\overline{p}_x}{\mathcal{M}}, \tag{57}$$

Thus, we are led to the linearised model

$$\frac{\partial}{\partial t}\tilde{n} + \frac{\partial}{\partial x}\left(n_0\frac{\tilde{\overline{p}}_x}{\mathcal{M}}\right) = -\frac{\hbar^2}{24}\frac{\partial^3}{\partial x^3}\left(n_0\frac{3v_F}{4p_F^3}\tilde{\overline{p}}_x\right), \tag{58}$$

$$\frac{\partial}{\partial t}(n_0\tilde{\overline{p}}_x) + \frac{\partial}{\partial x}\left(\frac{3}{4}p_F v_F\tilde{n}\right) + \mathcal{Q}n_0\frac{\partial}{\partial x}\tilde{\phi} = \frac{\hbar^2}{24}\frac{\partial^3}{\partial x^3}\left(\frac{3v_F}{8p_F}\tilde{n}\right), \tag{59}$$

where $\tilde{\phi}(\boldsymbol{r},t)$ is the first order electrostatic potential with respect to the perturbed density. Solving (58) and (59) simultaneously gives the plasmon dispersion relation

$$\omega(q) = \pm\left(\omega_p^2\frac{q}{k_F} + \frac{3}{4}v_F^2q^2 - \frac{\omega_p^2}{32}\frac{q^3}{k_F^3} + \nu\frac{\hbar^2q^4}{4\mathcal{M}^2}\right)^{1/2}, \tag{60}$$

where $\nu = -1/32$ is a numerical factor, which results from the contributions of both $\overline{J_{xxx}}$ and $\overline{T^x_{xxx}}$. The $\pm$ sign refers to each plasmon branch for forward and backward propagation. The two first terms are the classical contributions to the plasmon dispersion, in agreement with the result already found in (31), while the third term corresponds to a classical ($\hbar$ independent) correction. The quantum correction ($\sim\hbar^2$) is contained in the last term, and is owing to the Bohm potential [34]. It plays the role of a quantum pressure, and is responsible for tunneling and wave spreading effects. For Dirac plasmas, we thus find a negative Bohm contribution, contrary to that found for parabolic plasmas. Since the absolute of ν is rather small, corrections only becomes important for intermediate wave-number values.

V. STREAMING INSTABILITY

The kinetic model of (19) is now used to probe a plasmonic instability regime, using a specific configuration comprising two parallel layers of doped graphene, separated by a distance d. We consider the case $E_F \gg k_BT$, thus neglecting the contribution of holes. In one of the layers (*active* layer), a beam of electrons is injected by applying a potential difference to its edges. The drifting current that is formed, against the steady background electronic system, provides a mechanism of instability that is similar to that of two stream instability, extensively studied in the context of parabolic [35] and solid-state plasmas [36].

It can be shown, using (19), that the dielectric function for the composite system is given by

$$\begin{aligned}\epsilon(\boldsymbol{q},\omega) =& 1 + [e\mathcal{U}(q)]^2\Pi_\uparrow(\boldsymbol{q},\omega)\Pi_\downarrow(\boldsymbol{q},\omega)(1-e^{-2qd}) \\ &- e\mathcal{U}(q)\Big[\Pi_\uparrow(\boldsymbol{q},\omega) + \Pi_\downarrow(\boldsymbol{q},\omega)\Big],\end{aligned} \tag{61}$$

where the polarizability $\Pi_{\uparrow\downarrow}$ is calculated with (29) if we replace $W_0(\boldsymbol{k})$ by $W_{0\uparrow\downarrow}(\boldsymbol{k})$, denoting the equilibrium of

the *active* (↑) and *passive* (↓) layers. In the long wavelength limit, we find

$$\Pi_{\uparrow}(\boldsymbol{q},\omega) \simeq \frac{v_F k_{F\uparrow}}{\hbar\pi}\frac{q^2}{\omega^2} + \frac{v_F n_b}{\hbar k_b} \times \frac{q^2\sin^2\theta_b}{(\omega-\boldsymbol{v}_b\cdot\boldsymbol{q})^2 - \frac{v_F^2}{4k_b^2}q^4\sin^4\theta_b}, \quad (62)$$

$$\Pi_{\downarrow}(\boldsymbol{q},\omega) \simeq \frac{v_F k_{F\downarrow}}{\hbar\pi}\frac{q^2}{\omega^2}. \quad (63)$$

The first term in both (62) and (63) ($\sim q^2/\omega^2$) is due to the background doping electrons, while the second term in (62) comes from the contribution of the injected beam. Additionally, $k_\uparrow$ and $k_\downarrow$ are the Fermi wave-number of each layer, n_b and k_b denote the beam density and wave-number, $\boldsymbol{v}_b = v_F\boldsymbol{k}_b/k_b$ is the beam velocity and θ_b is the angle between $\boldsymbol{q}$ and $\boldsymbol{k}_b$.

The plasmon modes are given by the zeros of $\epsilon(\boldsymbol{q},\omega)$, of the form $\omega(\boldsymbol{q}) = \omega_r(\boldsymbol{q}) + i\omega_i(\boldsymbol{q})$. To solve (61), let us consider equally doped layers, *i.e.*, $k_\uparrow = k_\downarrow$. In this case, (61) is a sextic equation, with four stable ($\omega_i = 0$) and two unstable ($\omega_i \neq 0$) roots. The real roots represent the optical and acoustic modes, for backward and forward propagation, with well-known behaviour $\omega_{op} \sim \pm\sqrt{q}$ and $\omega_{ac} \sim \pm q$, in the long wavelength limit $q \to 0$. One of the complex roots represents a plasmon which is growing in time ($\omega_i > 0$), while the other is decaying ($\omega_i < 0$). In addiction, these solutions have degenerate real parts and symmetric imaginary parts. However, after a certain q_{max} in $\boldsymbol{q}-$space, the imaginary part of the unstable modes vanishes, and consequently, they become stable, while their corresponding real parts break into different branches (see Fig. 2).

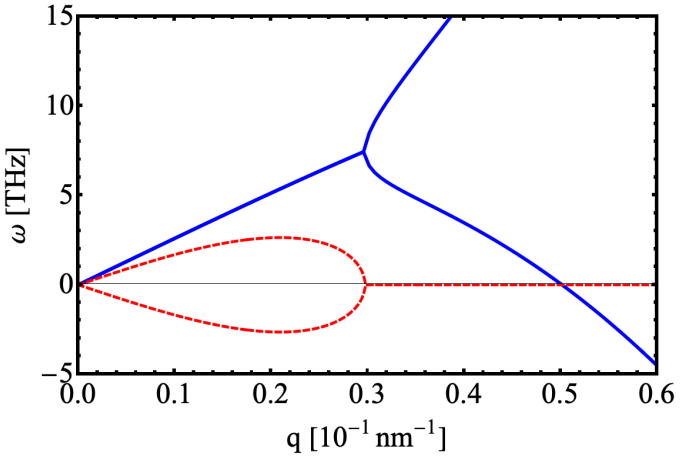

FIG. 2. Real part (blue lines) and imaginary part (red lines) of the unstable modes, $d = 0.15\lambda_F$, $n_b = 0.1n_0$, $k_b = 0.1k_F$, $\theta_b = \pi/4$ and $\varepsilon_r = 2.5$.

The factor $\sin^2\theta_b$ in (62) indicates that, for parallel plasmon and beam direction of propagation, the instability is suppressed. This strange behaviour is explained by the linear dispersion relation. In the described conditions, the exponential growing of the unstable mode happens because the charge fluctuations caused by the plasmon produce a net force, which feeds back the fluctuations, making them increase. However, this arguments fails when the plasmon direction of propagation is the same as the direction of the beam. Remember that Dirac electrons have a constant speed (v_F), and velocity align with momentum, *i.e.*, $\boldsymbol{v} = v_F\boldsymbol{p}/|\boldsymbol{p}|$. The momentum, in turn, can take any value. Therefore, for the parallel case, the charge fluctuations around the equilibrium densities only change the magnitude of the momentum, which does not affect the velocity, and the feedback does not occur. On the contrary, when both directions are not aligned, the fluctuations on the charge density are able to affect the direction of momentum, thus changing particles' velocities and allowing for a exponential growing of the wave.

VI. CONCLUSIONS

In the present work, we relied on a quantum kinetic formalism, based on the definition of phase-space functions through the Weyl transform, and derived a kinetic equation for the evolution of the Wigner function for the graphene quasi-particles.

We selected this formalism because it proves to be ideal to examine the semi-classical limit, hence allowing the construction of a set of hydrodynamical equations. Therefore, starting from a microscopic Hamiltonian, we were able to introduce the graphene odd kinetic term into an effective Schödinger equation, with the interacting potential given in the mean-field (or Hartree) approximation. Then, we constructed an hydrodynamical model for quantities by integrating the subsequent the Wigner equation in momentum space. The present formulation allowed to include, consistently, all quantum terms that contribute to dispersion in both the continuity and force equations. Those terms are usually neglected because the classical version of the Wigner equation (known as the Boltzmann or Vlasov equation) is commonly adopted. By keeping only the first of those contributions, a closed set of hydrodynamical equations was established. The closure relation came after a particular *ansatz* for the Wigner diagonal elements, interpreted as a shifted Fermi-sphere in momentum space, which depended explicitly on the hydrodynamical variables. The hydrodynamical set of equations enabled us to put forward an effective mass for Dirac particles in the hydrodynamical regime, for which analytical expression in several limiting cases of interest were derived.

In the end, we returned to the kinetic equation to examine an unstable plasmonic regime, in a particular double-sheet configuration of graphene layers. By comparing the results with the DS instability [16], often proposed as a solution to circumventing the THz-gap problem, we concluded that the present two stream instability

could deliver growth rates an order of magnitude higher, $\omega_i \in [0, 20]$ THz, for realistic experimental parameters. The real part of the frequency is also located in the THz range, conferring great pertinence to this research.

This work opened a line of investigation that should be followed in the future. The next natural requisite is the inclusion of scattering sources, as phonons and impurities, which are known to be important out of the zero-temperature limit. Interactions with magnetic fields can be introduced resorting to the vectorial Poisson equation, coupling the vector potential to the fluid current density. Additionally, quantum correlations can be treated, which will require the inclusion of the Wigner off-diagonal terms in the kinetic equations of interest.

[1] K. S. Novoselov, A. K. Geim, S. V. Morozov, D. Jiang, Y. Zhang, S. V. Dubonos, I. V. Grigorieva, and A. A. Firsov, Science **306**, 666 (2004).
[2] A. H. Castro Neto, F. Guinea, N. M. R. Peres, K. S. Novoselov, and A. K. Geim, Rev. Mod. Phys. **81**, 109 (2009).
[3] P. R. Wallace, Phys. Rev. **71**, 622 (1947).
[4] D. Rodrigo, O. Limaj, D. Janner, D. Etezadi, F. J. Garcia de Abajo, V. Pruneri, and H. Altug, Science **349**, 165168 (2015).
[5] S. Zeng, K. V. Sreekanth, J. Shang, T. Yu, C.-K. Chen, F. Yin, D. Baillargeat, P. Coquet, H.-P. Ho, A. V. Kabashin, and K.-T. Yong, Advanced Materials **27**, 6163 (2015).
[6] F. H. L. Koppens, D. E. Chang, and F. J. Garca de Abajo, Nano Letters **11**, 3370 (2011), pMID: 21766812.
[7] A. Agarwal, M. Vitiello, L. Viti, A. Cupolillo, and A. Politano, Nanoscale **10** (2018), 10.1039/C8NR01395K.
[8] S. Dai, Science **343**, 1125 (2014).
[9] Y. Lin, T. V. Williams, and J. W. Connell, The Journal of Physical Chemistry Letters **1**, 277 (2009).
[10] Y. Li, Z. Li, C. Chi, H. Shan, L. Zheng, and Z. Fang, Advanced Science **4**, 1600430 (2017).
[11] A. N. Grigorenko, M. Polini, and K. S. Novoselov, Nature Photonics **6**, 749 (2012).
[12] A. Geim and K. Novoselov, Nature materials **6**, 183 (2007).
[13] Y. Yang, Z. Shi, J. Li, and Z.-Y. Li, Photonics Research **4**, 65 (2016).
[14] F. Wang, Y. Zhang, C. Tian, C. Girit, A. Zettl, M. Crommie, and Y. R. Shen, Science **320**, 206 (2008).
[15] L. B. N. Laboratory, *Dirac Charge Dynamics in Graphene by Infrared Spectroscopy* (Lawrence Berkeley National Laboratory, 2008).
[16] P. Cosme and H. Terças, ACS Photonics **7**, 1375 (2020).
[17] V. Ryzhii, A. Satou, and T. Otsuji, Journal of Applied Physics - J APPL PHYS **101** (2007), 10.1063/1.2426904.
[18] R. Bistritzer and A. H. MacDonald, Phys. Rev. B **80**, 085109 (2009).
[19] D. Svintsov, V. Vyurkov, S. Yurchenko, T. Otsuji, and V. Ryzhii, Journal of Applied Physics **111**, 083715 (2012).
[20] U. Schwengelbeck, L. Plaja, L. Roso, and E. C. Jarque, Journal of Physics B: Atomic, Molecular and Optical Physics **33**, 1653 (2000).
[21] R. Jasiak, G. Manfredi, P.-A. Hervieux, and M. Haefele, New Journal of Physics **11**, 063042 (2009).
[22] T. V. Teperik, P. Nordlander, J. Aizpurua, and A. G. Borisov, Phys. Rev. Lett. **110**, 263901 (2013).
[23] E. Wigner, Phys. Rev. **40**, 749 (1932).
[24] G. e. a. Catarina, Handbook of Graphene , 177231 (2019).
[25] J. E. Moyal, Proc. Cambridge Phil. Soc. **45**, 99 (1949).
[26] A. L. Fetter and J. D. Walecka, *Quantum Theory of Many-Particle Systems* (McGraw-Hill, Boston, 1971).
[27] B. Wunsch, T. Stauber, F. Sols, and F. Guinea, New Journal of Physics **8**, 318 (2006).
[28] S. Das Sarma, E. Hwang, and Q. Li, Phys. Rev. B **80** (2009), 10.1103/PhysRevB.80.121303.
[29] S. Das Sarma and E. H. Hwang, Physical Review Letters **102** (2009), 10.1103/physrevlett.102.206412.
[30] C. Kittel, *Quantum Theory of Solids* (John Wiley and Sons, Inc, 1963).
[31] Y. Liu, R. Willis, K. Emtsev, and T. Seyller, Phys. Rev. B **78** (2008), 10.1103/PhysRevB.78.201403.
[32] B. Wunsch, T. Stauber, F. Sols, and F. Guinea, New Journal of Physics **8**, 318 (2006).
[33] A. J. Chaves, N. M. R. Peres, G. Smirnov, and N. A. Mortensen, Physical Review B **96** (2017), 10.1103/physrevb.96.195438.
[34] M.-J. Lee and Y.-D. Jung, Physics Letters A **381**, 636 (2017).
[35] R. Bharuthram, H. Saleem, and P. K. Shukla, Physica Scripta **45**, 512 (1992).
[36] B. B. Robinson and G. A. Swartz, Journal of Applied Physics **38**, 2461 (1967), https://doi.org/10.1063/1.1709928.